Signatures of chaos in the statistical distribution of conductance peaks in quantum dots

Y. Alhassid
Center for Theoretical Physics, Sloane Physics Laboratory, Yale University, New Haven, Connecticut 06520

C. H. Lewenkopf
Instituto de Física, Universidade de São Paulo, C.P. 66318, 05389-970 São Paulo, Brazil
and Instituto de Fisica, UERJ, R. Sao Francisco Xavier, 524, 20559-900 Rio de Janeiro, Brazil
(Received 1 May 1996)

Analytical expressions for the width and conductance peak distributions of irregularly shaped quantum dots in the Coulomb blockade regime are presented in the limits of conserved and broken time-reversal symmetry. The results are obtained using random matrix theory and are valid in general for any number of nonequivalent and correlated channels, assuming that the underlying classical dynamics of the electrons in the dot is chaotic or that the dot is weakly disordered. The results are expressed in terms of the channel correlation matrix, which for chaotic systems is given in closed form for both pointlike contacts and extended leads. We study the dependence of the distributions on the number of channels and their correlations. The theoretical distributions are in good agreement with those computed in a dynamical model of a chaotic billiard.
[S0163-1829(97)04912-6]

I. INTRODUCTION

One of the most interesting aspects of electron transport in submicrometer-scale devices is the interplay between quantum coherence and aperiodic but reproducible conductance fluctuations. Over the past decade the phenomenon of universal conductance fluctuations in disordered systems (where impurity scattering dominates) has been understood through the use of stochastic models. More recently, a new generation of experiments[1] was designed to measure conductance fluctuations in the ballistic regime where the dynamics of the electrons in the device is determined by the geometry of its boundary. The stochastic approach to these systems is justified by the underlying classical chaotic dynamics. This situation is distinct from the diffusive case, where the corresponding classical limit of the quantum problem is not fully understood.

In this paper we discuss the conductance fluctuations in quantum dots. These are semiconductor devices in which the electrons are confined to a two-dimensional region whose typical linear dimension is in the submicrometer range.[2–5] In particular we are interested in the Coulomb blockade regime where the leads are weakly coupled to the dot, either because the leads are very narrow, or because of potential barriers at the lead-dot interface.[2] The electrons inside the dot are characterized by isolated resonances whose width is smaller than their average spacing, and conductance occurs through resonant tunneling. As a consequence, the conductance is at a maximum when the Fermi energy matches a resonance energy of the electrons inside the dot and an additional electron tunnels into the dot. Such a system resembles the compound nucleus in its region of isolated resonances.[6] The macroscopic charging energy required to add an electron to a dot is determined by its capacitance C and is given by e^2/C. Since C is a constant that is determined essentially by the geometry of the dot, the conductance exhibits equally spaced oscillations as a function of the gate voltage (or Fermi energy). At low temperatures $\Gamma \ll kT < \Delta$ the width of the conductance peaks is $\sim kT$, but the heights exhibit order-of-magnitude variations.[3–5]

When the electron-impurity mean-free path is larger than the size of the dot, the classical dynamics of the electron inside the dot is determined by the scattering from the dot's boundary. Owing to small irregularities in the dot's shape, the electron displays chaotic motion, and its quantum transport through the dot can be described by a statistical S-matrix theory.[7] Since the Coulomb blockade regime is dominated by resonances, the conductance peaks can be used to probe the chaotic properties of the underlying resonance wave-functions. A statistical theory of the conductance peaks was originally developed in Ref. 8. By using R-matrix theory,[9,10] the conductance peak amplitude was expressed in terms of the electronic resonance wave function across the contact region between the dot and the leads. When the dynamics of the electron inside the dot is chaotic, the fluctuations of the wave-function inside the dot are assumed to be well described by random matrix theory (RMT). In Ref. 8 the conductance distribution was derived in closed form for one-channel leads. These results were rederived in Ref. 11, and later extended to the case of two-channel leads in the absence of time-reversal symmetry[12] through the use of the supersymmetry technique.[13] However, the calculations required by this technique become too complicated to apply in the general case of any number of possibly correlated and/or nonequivalent channels.

The conductance distributions for one-channel leads were recently measured[14,15] and found to be in agreement with theory for both cases of conserved and broken time-reversal symmetry. This indicates that the dephasing effect, which plays an important role in open dots,[16,17] is of little importance for closed dots.

In this paper we discuss in detail the width and conductance peak distributions for leads with any number of channels that are in general correlated and nonequivalent. Exact

closed expressions for these distributions are derived for both cases of conserved and broken time-reversal symmetry.[18] We find that these distributions are entirely characterized by the eigenvalues of the channel correlation matrices M^l and M^r in the left and right leads, respectively. The strength of our approach is in its simplicity, since it relies solely on standard RMT techniques. To test our predictions we compare our analytical findings to numerical simulations of a chaotic dynamical model, the conformal billiard.[19] Statistical width and conductance distributions of one-channel leads were recently studied in detail in this model.[20] Although our paper deals mainly with ballistic dots whose classical dynamics is chaotic, our results should also be valid in the diffusive regime of weakly disordered dots, where random matrix theory is applicable.

We note that the partial width amplitude is analogous to the wave-function amplitude at any given point. Therefore our width distributions can also be tested by microwave cavity experiments,[21–23] where the intensities are measured at several points that are spatially correlated. As a side result we obtain the joint distribution of a chaotic wave-function amplitude at several spatial points. From this distribution it is straightforward to calculate the joint distribution of the wave-function intensities.

This paper is organized as follows: In Sec. II we briefly review the conductance in quantum dots in their Coulomb blockade regime. In Sec. III we discuss the statistical model and derive analytic results for the partial and total width distributions in each lead, for the channel correlation matrix, and for the conductance distribution. We investigate the variation of these distributions as a function of the number of channels and their sensitivity to the degree of correlation between them. Those findings are compared in Sec. IV with numerical results obtained for the conformal billiard. Finally, in Sec. V we discuss the validity of our assumptions in the the context of typical experiments.

II. CONDUCTANCE IN QUANTUM DOTS

In this section we briefly review the formalism and introduce the notation used throughout this paper. In particular, we express the conductance peak heights in terms of the channel and resonance wave-functions of the dot.

For $\Gamma \ll kT \ll \Delta$, which is typical of many experiments,[3] the observed on-resonance conductance peak amplitude is given by[24,25]

$$G_\lambda = \frac{e^2}{h}\frac{\pi}{2kT} g_\lambda, \quad \text{with} \quad g_\lambda = \frac{\Gamma_\lambda^l \Gamma_\lambda^r}{\Gamma_\lambda^l + \Gamma_\lambda^r}, \tag{1}$$

where $\Gamma_\lambda^{l(r)}$ is the partial decay width of the resonance λ into the left (right) lead. Since each lead can support several open channels we have $\Gamma_\lambda^{l(r)} = \sum_c \Gamma_{c\lambda}^{l(r)}$, where $\Gamma_{c\lambda}^{l(r)}$ is the partial width to decay into channel c in the left (right) lead.

In the R-matrix formalism,[10] the partial widths are related to the resonance wave-function inside the dot. More specifically, introducing the partial amplitudes $\gamma_{c\lambda}$, such that $\Gamma_{c\lambda} = |\gamma_{c\lambda}|^2$, one can write

$$\gamma_{c\lambda} = \sqrt{\frac{\hbar^2 k_c P_c}{m}} \int dS \Phi_c^*(\boldsymbol{r}) \Psi_\lambda(\boldsymbol{r}). \tag{2}$$

Here $\Psi_\lambda(\boldsymbol{r})$ is the λth resonance wave-function in the dot, $\Phi_c(\boldsymbol{r})$ is the transverse wave-function in the lead that corresponds to an open channel c, and the integral is taken over the contact area between the lead and the dot. k_c and P_c are the longitudinal wave number and penetration factor in channel c, respectively.

Equation (2) shows that the contributions to the partial width amplitude from the internal and external regions of the dot factorize. The information from the external region is contained in k_c and P_c. These quantities are determined by the wave dynamics in the leads and are nonuniversal. They affect the average widths and enter explicitly in the correlation matrix M. However, the fluctuation properties of the conductance are generic and depend only on the statistical properties of the electronic wave-function at the dot-lead boundary inside the barrier region.

A different physical modeling of a quantum dot assumes pointlike contacts, and each lead is composed of several such point contacts.[11,12] In this model the conductance peak is also given by Eq. (1) with each point contact $\boldsymbol{r}_c$ considered as one channel. The corresponding partial width is[11]

$$\gamma_{c\lambda} = \sqrt{\frac{\alpha_c \mathcal{A}\Delta}{\pi}} \Psi_\lambda(\boldsymbol{r}_c), \tag{3}$$

where $\mathcal{A}$ is the area of the dot, Δ is the mean spacing, and α_c is a dot-lead coupling parameter.

Both models can be treated by our formalism, as becomes apparent from the following considerations. A resonance eigenfunction with eigenenergy E can be approximated by an expansion in a fixed basis ρ_μ of wave-functions with the given energy E inside the dot

$$\Psi_\lambda(\boldsymbol{r}) = \sum_\mu \psi_{\lambda\mu} \rho_\mu(\boldsymbol{r}). \tag{4}$$

The sum over μ is truncated at N basis states (N is much larger than the number of open channels). The partial width in channel c can then be expressed by the scalar product

$$\gamma_{c\lambda} = \langle \boldsymbol{\phi}_c | \boldsymbol{\psi}_\lambda \rangle \equiv \sum_\mu \phi_{c\mu}^* \psi_{\lambda\mu}, \tag{5}$$

where

$$\phi_{c\mu} \equiv \sqrt{\frac{\hbar^2 k_c P_c}{m}} \int dS \Phi_c^*(\boldsymbol{r}) \rho_\mu(\boldsymbol{r}) \tag{6}$$

for the extended leads model, and

$$\phi_{c\mu} \equiv \sqrt{\frac{\alpha_c \mathcal{A}\Delta}{\pi}} \rho_\mu^*(\boldsymbol{r}_c) \tag{7}$$

for the point contact model. Thus, we are led to similar formulations of both the extended leads and pointlike contact problems; in the corresponding N-dimensional space the partial width amplitudes of a level are simply the projections of its corresponding eigenstate vector $\boldsymbol{\psi}_\lambda$ on the channel vectors $\boldsymbol{\phi}_c$. The only difference between the two models is the explicit expression for the channel vector $\boldsymbol{\phi}_c$. We note that the scalar product (5) (used throughout this paper) is different from the original scalar product defined in the spatial region extended by the dot.

III. STATISTICAL MODEL

Because the dot's shape is irregular, the motion of the electron inside the dot is expected to be chaotic. In Ref. 8 we developed a statistical theory of the conductance peaks by assuming that the vectors $\boldsymbol{\psi}_\lambda$ that correspond to the resonance wave-functions inside the dot have the same statistical properties as the eigenvectors of a random matrix ensemble. Here we study the limits of conserved time-reversal symmetry, corresponding to the Gaussian orthogonal ensemble (GOE), and of broken time-reversal symmetry, corresponding to the Gaussian unitary ensemble (GUE). The transition from one symmetry to another occurs when an external magnetic field is applied. The width distribution (or equivalently the wave-function intensity distribution) was derived in the crossover regime between symmetries for the case of one channel leads only.[26]

A. The joint distribution of partial width amplitudes

In RMT the eigenvector $\boldsymbol{\psi}\equiv(\psi_1,\psi_2,\ldots,\psi_N)$ (here and in the following we omit the eigenvector label λ) is distributed randomly[27] on a sphere $P(\boldsymbol{\psi})\propto\delta(\Sigma_{\mu=1}^{N}|\psi_\mu|^2-1)$. The joint distribution of the partial width amplitudes $\boldsymbol{\gamma}=(\gamma_1,\gamma_2,\ldots,\gamma_\Lambda)$ for Λ channels is then given by

$$P(\boldsymbol{\gamma})=\frac{\Gamma(\beta N/2)}{\pi^{\beta N/2}}\int D[\boldsymbol{\psi}]\left[\prod_{c=1}^{\Lambda}\delta(\gamma_c-\langle\boldsymbol{\phi}_c|\boldsymbol{\psi}\rangle)\right]\delta\left(\sum_{\mu=1}^{N}|\psi_\mu|^2-1\right), \tag{8}$$

where $D[\boldsymbol{\psi}]\equiv\Pi_{\mu=1}^{N}d\psi_\mu$ for the GOE and $D[\boldsymbol{\psi}]\equiv\Pi_{\mu=1}^{N}d\psi_\mu^*d\psi_\mu/2\pi i$ for the GUE. To evaluate Eq. (8) we transform the Λ channels to a new set of orthonormal channels $\hat{\boldsymbol{\phi}}_c$:

$$\boldsymbol{\phi}_c=\sum_{c'}\hat{\boldsymbol{\phi}}_{c'}F_{c'c},\quad\text{with }\langle\hat{\boldsymbol{\phi}}_c|\hat{\boldsymbol{\phi}}_{c'}\rangle=\delta_{cc'}. \tag{9}$$

We then take advantage of the invariance of the corresponding Gaussian ensemble under an orthogonal (unitary) transformation to rotate the eigenvector $\boldsymbol{\psi}$ such that its first Λ components are along the new orthonormal channels. Denoting by $\mathcal{O}$ the orthogonal (unitary) matrix whose first Λ rows are the orthonormal vectors $\hat{\boldsymbol{\phi}}_c(c=1,\ldots,\Lambda)$, we change variables in (5) to $\hat{\psi}_\mu=\Sigma_\nu\mathcal{O}_{\mu\nu}\psi_\nu$. Using $\hat{\psi}_c=\langle\hat{\boldsymbol{\phi}}_c|\boldsymbol{\psi}\rangle$ we find

$$P(\boldsymbol{\gamma})=\frac{\Gamma(\beta N/2)}{\pi^{\beta N/2}}\int\left(\prod_{c=1}^{\Lambda}d\hat{\psi}_c\right)\left(\prod_{\mu=\Lambda+1}^{N}d\hat{\psi}_\mu\right)\left[\prod_{c=1}^{\Lambda}\delta(\gamma_c-F_{c'c}\hat{\psi}_{c'})\right]\delta\left(\sum_{c=1}^{\Lambda}|\hat{\psi}_c|^2+\sum_{\mu=\Lambda+1}^{N}|\hat{\psi}_\mu|^2-1\right). \tag{10}$$

The integration over these first Λ components is now easily done and gives

$$P(\boldsymbol{\gamma})=\frac{\Gamma(\beta N/2)}{\pi^{\beta N/2}|\det F|}\int D[\hat{\boldsymbol{\psi}}]\,\delta\left(\hat{\boldsymbol{\gamma}}^\dagger\hat{\boldsymbol{\gamma}}+\sum_{\mu=\Lambda+1}^{N}|\hat{\psi}_\mu|^2-1\right), \tag{11}$$

where $\hat{\gamma}_c\equiv\langle\hat{\boldsymbol{\phi}}_c|\boldsymbol{\psi}\rangle=\Sigma_{c'}\gamma_{c'}F^{-1*}_{c'c}$ are the partial widths to decay to the new channels and the metric is as before but excluding the first Λ components of $\boldsymbol{\psi}$. Finally, the latter integral is easily done by introducing spherical coordinates in the $(N-\Lambda)$-dimensional space. We obtain

$$P(\boldsymbol{\gamma})=\frac{\Gamma(\beta N/2)}{\pi^{\beta\Lambda/2}\Gamma(\beta(N-\Lambda)/2)|\det F|}\times[1-\boldsymbol{\gamma}^\dagger(F^\dagger F)^{-1}\boldsymbol{\gamma}]^{\beta(N-\Lambda)/2-1}. \tag{12}$$

For $\Lambda\ll N$ and in the limit $N\to\infty$, we recover a simplified expression

$$P(\boldsymbol{\gamma})=(\det M)^{-\beta/2}e^{-(\beta/2)\boldsymbol{\gamma}^\dagger M^{-1}\boldsymbol{\gamma}}, \tag{13}$$

where the matrix $M\equiv(NF^\dagger F)^{-1}$ is just the metric defined in terms of the original channels

$$M_{cc'}=\frac{1}{N}\langle\boldsymbol{\phi}_c|\boldsymbol{\phi}_{c'}\rangle. \tag{14}$$

The distribution (13) is normalized with the measure $D[\boldsymbol{\gamma}]\equiv\Pi_{c=1}^{\Lambda}(d\gamma_c/\sqrt{2\pi})$ for the GOE and $D[\boldsymbol{\gamma}]\equiv\Pi_{c=1}^{\Lambda}(d\gamma_c^*d\gamma_c/2\pi i)$ for the GUE. Note that for both ensembles the joint partial width amplitudes distribution is Gaussian, the main difference being that the partial amplitudes are real for the GOE and complex for the GUE. Such a Gaussian distribution is also obtained by assuming that the distribution is form invariant under an orthogonal (unitary) transformation.[28]

It follows from Eq. (13) that the matrix M is just the correlation matrix of the partial widths

$$M_{cc'}=\overline{\gamma_c^*\gamma_{c'}}. \tag{15}$$

In general the channels are correlated ($M_{cc'}\neq0$) and nonequivalent (their average partial widths are different). Ac-

cording to Eq. (14) this is equivalent to assuming channels that are nonorthogonal and have nonequal norms.

B. The channel correlation matrix *M*

We shall now derive explicit expressions for the correlation matrix M in a chaotic quantum dot. Using Eq. (14) and the definition of the scalar product (5) we find

$$M_{cc'}=\frac{\hbar^2}{2m}\sqrt{k_c k_{c'} P_c P_{c'}}\int dS\int dS'\,\Phi_c^*(\boldsymbol{r}) \times\left[\frac{1}{N}\sum_\mu \rho_\mu(\boldsymbol{r})\rho_\mu(\boldsymbol{r}')\right]\Phi_c(\boldsymbol{r}'). \tag{16}$$

We first discuss the case where there is no magnetic field so that the motion inside the dot is that of a free particle. A resonance eigenstate inside the dot at energy $E=\hbar^2k^2/2m$ can then be expanded in a basis of free particle states at the given energy E. Since RMT is applicable on a local energy scale, this is the fixed basis ρ_μ for which the eigenvector coefficients ψ_μ are distributed randomly (on the sphere). Using polar coordinates, such a basis of free waves is given by $\rho_\mu(\boldsymbol{r})\propto J_\mu(kr)\exp(i\mu\theta)$ with $\mu=0,\pm1,\pm2,\ldots$, where J_μ are Bessel functions of the first kind. Denoting by N the number of such waves on the energy shell, we find

$$\frac{1}{N}\sum_\mu \rho_\mu^*(\boldsymbol{r})\rho_\mu(\boldsymbol{r}')=\frac{1}{\mathcal{A}}\sum_\mu J_\mu(kr)J_\mu(kr')\mathrm{e}^{i\mu(\theta'-\theta)} =\frac{1}{\mathcal{A}}J_0(k|\boldsymbol{r}-\boldsymbol{r}'|), \tag{17}$$

where we have used the addition theorem for the Bessel functions.[29] A similar relation holds if we choose a plane-wave basis $\rho_\mu(\boldsymbol{r})=\mathcal{A}^{-1/2}\exp(i\boldsymbol{k}_\mu\cdot\boldsymbol{r})$ at a fixed energy $\hbar^2k^2/2m$ but with random orientation of $\boldsymbol{k}_\mu$ and use the integral representation of J_0. With the help of Eq. (17) we obtain for the correlation matrix

$$M_{cc'}=\frac{\hbar^2}{2m\mathcal{A}}\sqrt{k_c k_{c'} P_c P_{c'}}\int dS\int dS'\,\Phi_c^*(\boldsymbol{r}) \times J_0(k|\boldsymbol{r}-\boldsymbol{r}'|)\Phi_c(\boldsymbol{r}'), \tag{18}$$

for extended leads, while for the point contact model we find

$$M_{cc'}=\frac{\sqrt{\alpha_c\alpha_c}\Delta}{\pi}J_0(k|\boldsymbol{r}_c-\boldsymbol{r}_c'|). \tag{19}$$

We remark that Eq. (19) is equivalent to $C(k|\Delta\boldsymbol{r}|)\equiv\overline{\Psi^*(\boldsymbol{r})\Psi(\boldsymbol{r}')}/\overline{|\Psi(\boldsymbol{r})|^2}=J_0(k|\boldsymbol{r}-\boldsymbol{r}'|)$. This result was first derived in Ref. 30 based on the assumption that the Wigner function of a classically chaotic system is microcanonical on the energy surface. It was recently studied extensively in the Africa billiard[31] (this billiard is discussed in Sec. IV). We note, however, that in these references the average is taken for a fixed wave-function over a local spatial region around $(\boldsymbol{r}+\boldsymbol{r}')/2$, while we average over eigenstates.

When an external magnetic field B is present, the underlying classical dynamics undergoes a transition from chaotic to integrable as the field gets stronger, irrespective of the billiard's shape. In the present work, however, we only discuss the case of weak fields for which the motion is chaotic, and we are interested in the transition from orthogonal to unitary symmetry. While in the unitary case the wave-functions become complex, the arguments that lead to Eq. (17) are still valid and the wave-function correlator $C(k|\Delta\boldsymbol{r}|)$ is unchanged. For our studies to be experimentally relevant, it is important to have a range of values of the magnetic field for which time-reversal symmetry is broken but the underlying classical dynamics is still chaotic.[32] We shall discuss this issue in Sec. V.

The wave-function correlation $C(k|\Delta\boldsymbol{r}|)$ was also derived for weakly disordered systems using the supersymmetry technique[33] for the unitary and orthogonal symmetries. Reference 33 also includes an expression for the joint probability distribution for the intensity of an eigenfunction at two different points. We remark that the joint distribution of the wave-function amplitude at Λ points $\boldsymbol{r}_c$ ($c=1,2,\ldots,\Lambda$) is a special case of Eq. (13) obtained for $\gamma_{c\lambda}\equiv\Psi_\lambda(\boldsymbol{r}_c)$ [see the point contact case (3) except that the points $\boldsymbol{r}_c$ can be chosen anywhere within the dot and not only on its boundary]. We then obtain

$$P(\Psi_\lambda(\boldsymbol{r}_1),\Psi_\lambda(\boldsymbol{r}_2),\ldots,\Psi_\lambda(\boldsymbol{r}_\Lambda))=(\det M)^{-\beta/2}\exp\left[-\frac{\beta}{2}\sum_{cc'=1}^{\Lambda}\Psi_\lambda^*(\boldsymbol{r}_c)(M^{-1})_{cc'}\Psi_\lambda(\boldsymbol{r}_{c'})\right], \tag{20}$$

where $M_{cc'}=\mathcal{A}^{-1}J_0(k|\boldsymbol{r}_c-\boldsymbol{r}_c'|)$. The distributions of Ref. 33 are easily obtained from Eq. (20) when $\Lambda=2$.[34]

C. Total width distribution

We calculate next the total width distribution $P(\Gamma)$ in a given lead that supports Λ channels and is characterized by a correlation matrix M. This distribution is relevant more generally for resonant scattering by complex objects.[21,22,35] For a dot with reflection symmetry $\Gamma^l=\Gamma^r\equiv\Gamma$ the conductance peak g in Eq. (1) is proportional to Γ. However, such dots are difficult to fabricate. Instead, one can in principle measure these distributions for very asymmetric leads where the conductance peak is dominated by the lead with the smaller width.

Using $\Gamma=\Sigma_c|\gamma_c|^2=\boldsymbol{\gamma}^\dagger\boldsymbol{\gamma}$, the characteristic function of $P(\Gamma)$ is given by

$$\widetilde{P}(t)=\int_0^\infty d\Gamma\,\exp(it\Gamma)P(\Gamma)=\int D[\boldsymbol{\gamma}]\exp(it\boldsymbol{\gamma}^\dagger\boldsymbol{\gamma})P(\boldsymbol{\gamma}). \tag{21}$$

Since $P(\boldsymbol{\gamma})$ is a Gaussian, we readily obtain $\widetilde{P}(t)=[\det(I-2iMt/\beta)]^{-\beta/2}$. The distribution itself is then given by an inverse Fourier transform

$$P(\Gamma)=\frac{1}{2\pi}\int_{-\infty}^{\infty}dt\,\frac{e^{-it\Gamma}}{[\det(I-2itM/\beta)]^{\beta/2}}. \tag{22}$$

The matrix M is Hermitean and positive definite (since $\boldsymbol{x}^\dagger M\boldsymbol{x}=|\boldsymbol{x}\cdot\boldsymbol{\gamma}|^2>0$ for any $\boldsymbol{x}\neq 0$) and therefore its eigenvalues w_c^2 are all positive. According to Eq. (22), $P(\Gamma)$ depends only on w_c^2. This is a consequence of the invariance of Γ under a orthogonal (unitary) transformation of the Λ partial width amplitudes.

We first discuss the simpler GUE case, for which the integrand has poles $-i/w_c^2$ along the negative imaginary axis. Taking a contour integration along the real line and a half circle that encloses all the poles in the lower half of the plane, we can calculate Eq. (22) by residues. Assuming that all eigenvalues of M are nondegenerate, the poles are all simple and we find

$$P_{\mathrm{GUE}}(\Gamma)=\left(\prod_c\frac{1}{w_c^2}\right)\sum_{c=1}^{\Lambda}\left[\prod_{c'\neq c}\left(\frac{1}{w_{c'}^2}-\frac{1}{w_c^2}\right)\right]^{-1}e^{-\Gamma/w_c^2}. \tag{23}$$

The distribution $P_{\mathrm{GUE}}(\Gamma)$ given by Eq. (23) must be positive, which can be directly verified by using the concavity of the exponential function.

For two channels ($\Lambda=2$) that are in general nonequivalent ($M_{11}\neq M_{22}$) and correlated ($M_{12}\neq 0$), the eigenvalues are given by $w_{1,2}^2=(M_{11}+M_{22})/2\pm\sqrt{[(M_{11}-M_{22})/2]^2+|M_{12}|^2}$. Equation (23) reduces then to

$$P_{\mathrm{GUE}}^{\Lambda=2}(\hat{\Gamma})=\frac{2a_+}{\sqrt{a_-^2+|f|^2}}e^{-2a_+^2\hat{\Gamma}/(1-|f|^2)}\times\sinh\left(\frac{2a_+\sqrt{a_-^2+|f|^2}}{1-|f|^2}\hat{\Gamma}\right), \tag{24}$$

where $\hat{\Gamma}=\Gamma/\overline{\Gamma}$ is the width in units of its average value, $f=M_{12}/\sqrt{M_{11}M_{22}}$ measures the degree of correlation between the two channels, and $a_\pm=1/2(\sqrt{M_{11}/M_{22}}\pm\sqrt{M_{22}/M_{11}})$ are dimensionless parameters such that for equivalent channels $a_+=1$ and $a_-=0$. In the latter case, we reproduce the result of Ref. 12.

For degenerate eigenvalues, we can calculate Eq. (22) by using the residue formula for higher-order poles. Alternatively we can slightly break the degeneracy of the eigenvalues by η and take the limit $\eta\to 0$. For example, for two channels Eq. (23) gives $P(\Gamma)=(e^{-\Gamma/w_1^2}-e^{-\Gamma/w_2^2})/(w_2^2-w_1^2)$. By taking $w_2^2=w_1^2+\eta$, in the limit $\eta\to 0$ we recover

$$P(\Gamma)=\frac{\Gamma}{w^4}e^{-\Gamma/w^2}, \tag{25}$$

which is the χ^2 distribution in four degrees of freedom. More generally, when all Λ channels are uncorrelated and equivalent ($M=w^2I$) we recover the well-known χ^2 distribution in 2Λ degrees of freedom[6]

$$P_{\mathrm{GUE}}^{(0)}(\Gamma)=\frac{1}{w^{2\Lambda}(\Lambda-1)!}\Gamma^{\Lambda-1}e^{-\Gamma/w^2}. \tag{26}$$

We have denoted this limiting distribution in Eq. (26) by $P_{\mathrm{GUE}}^{(0)}$ as it will serve as our reference distribution against which to compare the distributions in the general case of correlated and/or nonequivalent channels.

For the GOE case, the integral of Eq. (22) is more difficult to evaluate since the singularities of the integrand along the negative imaginary axis $t=-i\tau$ are of the type $(\tau-1/2w_c^2)^{-1/2}$. In this case the semicircular part of the contour (in the lower half of the plane) is deformed, going up and then down along the negative imaginary axis so as to exclude all the singularities. When going around a singularity of this type the integrand changes sign. Therefore, after sorting the inverse eigenvalues of M in ascending order $w_1^{-2}<w_2^{-2}<\cdots$, we have

$$P_{\mathrm{GOE}}(\Gamma)=\frac{1}{\pi 2^{\Lambda/2}}\left(\prod_c\frac{1}{w_c}\right)\sum_{m=1}\int_{1/2w_{2m-1}^2}^{1/2w_{2m}^2}d\tau\times\frac{e^{-\Gamma\tau}}{\sqrt{\prod_{r=1}^{2m-1}[\tau-(1/2w_r^2)]\prod_{s=2m}^{\Lambda}[(1/2w_s^2)-\tau)]}}, \tag{27}$$

where for an odd number of channels Λ, we define $1/2w_{\Lambda+1}^2\to\infty$. The integrand of each term on the right-hand side of Eq. (27) is singular at the two end points of the integration interval, but this singularity is integrable. For the case of two channels that are in general nonequivalent but correlated, Eq. (27) reduces to

$$P_{\mathrm{GOE}}^{\Lambda=2}(\hat{\Gamma})=\frac{a_+}{\sqrt{1-|f|^2}}e^{-a_+^2\hat{\Gamma}/(1-|f|^2)}I_0\left(\frac{a_+\sqrt{a_-^2+|f|^2}}{1-|f|^2}\hat{\Gamma}\right), \tag{28}$$

where f and $a_\pm$ are defined as before [see text following Eq. (24)] and I_0 is the Bessel function of order zero. The case of equivalent channels is obtained in Eq. (28) by substituting $a_+=1$ and $a_-=0$.

The reference distribution $P_{\mathrm{GOE}}^{(0)}$, defined as before for the case where all Λ channels are equivalent and uncorrelated, is found directly from Eq. (22) to be the χ^2 distribution in Λ degrees of freedom[36,8]

$$P_{\mathrm{GOE}}^{(0)}(\Gamma)=\frac{1}{(2w^2)^{\Lambda/2}(\Lambda/2-1)!}\Gamma^{\Lambda/2-1}e^{-\Gamma/2w^2}. \tag{29}$$

The top panels (a) and (b) in Fig. 1 show the width distributions for a two-channel lead in the GOE statistics. The left panel is for equivalent channels ($M_{22}/M_{11}=1$) and for various degrees of correlations $f=0.25$, 0.5, 0.75, and 0.95. The right panel is for uncorrelated ($f=0$) but nonequivalent channels: $M_{22}/M_{11}=2$, 3, 4, and 5. The bottom

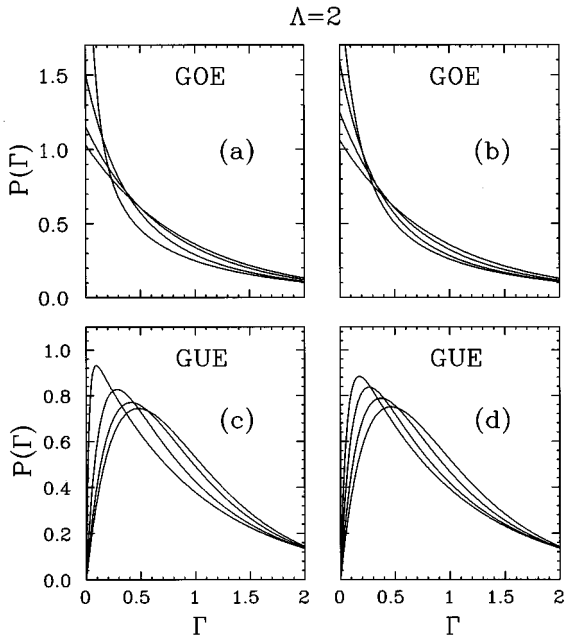

FIG. 1. Total width distributions $P(\Gamma)$ for a two-channel lead. Panels (a),(b) correspond to the orthogonal symmetry and (c),(d) to the unitary symmetry. $P(\Gamma)$ for equivalent but correlated channels with $f=0.25,\ 0.5,\ 0.75$, and 0.95 are shown in (a) and (c), while $P(\Gamma)$ for uncorrelated but nonequivalent channels with $M_{22}/M_{11}=2,\ 3,\ 4,\ 5$ are shown in (b) and (d). Descending values of f (or M_{22}/M_{11}) correspond to distributions that extend to larger values of Γ.

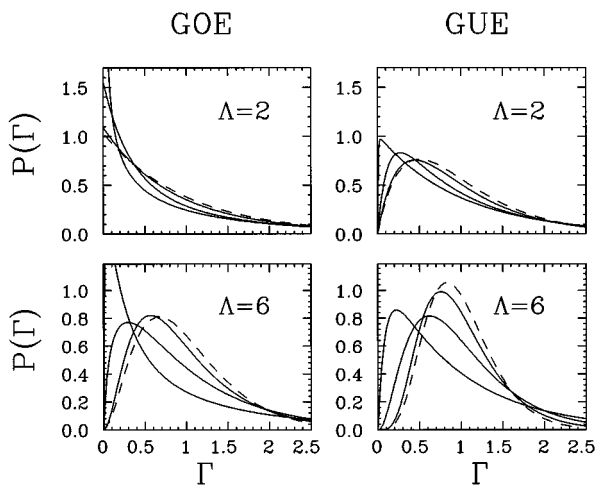

FIG. 2. Total width distributions for a Λ-point lead ($\Lambda=2,\ 6$) with $k|\Delta \boldsymbol{r}|=0.25,\ 1$, and 4 in a quantum dot with orthogonal symmetry (GOE) and with unitary symmetry (GUE). The dashed lines correspond to uncorrelated and equivalent channels. Increasing values of $k|\Delta \boldsymbol{r}|$ correspond to curves that approach the case of uncorrelated channels.

panels (c) and (d) in Fig. 1 are similar to (a) and (b) except that they correspond to the GUE case. We note that all figures display the normalized total width $\Gamma/\overline{\Gamma}$ as Γ.

The correlation matrix in the point contact model is fully determined by $k|\Delta \boldsymbol{r}|$ and the number of channels Λ. The left panels in Fig. 2 show the GOE width distributions for $k|\Delta \boldsymbol{r}|=0.25,\ 1,\ 4$ and for different number of channels $\Lambda=2$ and 6. The right panels of Fig. 2 show similar results but for the GUE statistics. The deviation of the width distribution from the one that corresponds to equivalent and uncorrelated channels (dashed lines in Fig. 2) becomes larger as the number of channels increases for a given $k|\Delta \boldsymbol{r}|$.

D. Conductance peaks distribution

To calculate the conductance distribution $P(g)$ in the general case, we assume that the left and right leads are far from each other and thus uncorrelated.[37] The left and right leads are characterized by their own correlation matrix M^l and M^r, respectively. Under this assumption,

$$P(g)=\int d\Gamma^l d\Gamma^r \delta\left(g-\frac{\Gamma^l\Gamma^r}{\Gamma^l+\Gamma^r}\right)P(\Gamma^l)P(\Gamma^r), \quad (30)$$

where $P(\Gamma)$ is given by Eq. (23) in the unitary case and by Eq. (27) in the orthogonal case.

The distribution $P(g)$ can be evaluated by the following identity

$$\int_0^\infty d\Gamma_1 \int_0^\infty d\Gamma_2 e^{-\Gamma_1/\delta_1}e^{-\Gamma_2/\delta_2}\delta\left(g-\frac{\Gamma_1\Gamma_2}{\Gamma_1+\Gamma_2}\right)=4ge^{-(1/\delta_1+1/\delta_2)g}\left[K_0\left(\frac{2g}{\sqrt{\delta_1\delta_2}}\right)+\frac{1}{2}\left(\sqrt{\frac{\delta_2}{\delta_1}}+\sqrt{\frac{\delta_1}{\delta_2}}\right)K_1\left(\frac{2g}{\sqrt{\delta_1\delta_2}}\right)\right], \quad (31)$$

provided $\delta_1,\delta_2>0$. To obtain this identity we have used the integral representation of the Bessel function $K_\nu(z)=1/2(z/2)^\nu\int_0^\infty dt\, t^{-\nu-1}e^{-t-z^2/4t}$.

For the unitary case, Eqs. (23) and (31) give

$$P_{\rm GUE}(g)=16g\left(\prod_c \frac{1}{v_c^2}\right)\left(\prod_d \frac{1}{w_d^2}\right)\sum_{c,d}^{\Lambda,\Lambda'}\left[\prod_{c'\neq c}\left(\frac{1}{v_{c'}^2}-\frac{1}{v_c^2}\right)\prod_{d'\neq d}\left(\frac{1}{w_{d'}^2}-\frac{1}{w_d^2}\right)\right]^{-1}$$
$$\times e^{-(1/v_c^2+1/w_d^2)g}\left[K_0\left(\frac{2g}{v_c w_d}\right)+\frac{1}{2}\left(\frac{v_c}{w_d}+\frac{w_d}{v_c}\right)K_1\left(\frac{2g}{v_c w_d}\right)\right], \quad (32)$$

where v_c^2 and w_d^2 are the eigenvalues of the left and right lead correlation matrices M^l and M^r, respectively. For one-channel leads with $\overline{\Gamma^l}=\overline{\Gamma^r}$ (i.e., $v_1=w_1$), Eq. (32) reproduces the results of Refs. 8 and 11, while the distribution of Ref. 12 is obtained

for two- (equivalent) channel leads whose matrices are related by an overall asymmetry factor $M^r = aM^l$.

A similar calculation for the orthogonal limit gives

$$P_{\mathrm{GOE}}(g) = \frac{4g}{\pi^2 2^{\Lambda}} \left(\prod_c \frac{1}{v_c} \right) \left(\prod_d \frac{1}{w_d} \right) \sum_{m,m'} \int_{1/2v_{2m-1}^2}^{1/2v_{2m}^2} d\tau \int_{1/2w_{2m'-1}^2}^{1/2w_{2m'}^2} d\tau' e^{-(\tau-\tau')g} \times \frac{K_0(2g\sqrt{\tau\tau'}) + \frac{1}{2}\left(\sqrt{\frac{\tau}{\tau'}} + \sqrt{\frac{\tau'}{\tau}} \right) K_1(2g\sqrt{\tau\tau'})}{\left[\prod_{r=1}^{2m-1} (\tau - 1/2v_r^2) \prod_{s=2m}^{\Lambda} (1/2v_s^2 - \tau) \prod_{r'=1}^{2m'-1} (\tau' - 1/2w_{r'}^2) \prod_{s'=2m'}^{\Lambda} (1/2w_{s'}^2 - \tau') \right]^{1/2}}. \tag{33}$$

Figure 3 shows the GOE (left) and GUE (right) conductance peak distribution (33) and (32), respectively, for symmetric Λ-point leads with $k|\Delta \boldsymbol{r}| = 0.25,\ 1,\ 4$ and for $\Lambda = 2$ and 6 (the same cases shown in Fig. 2). In all figures displaying $P(g)$, g denotes the normalized conductance $g/\overline{g}$. By comparing Fig. 3 with Fig. 2 we conclude that, as Λ increases, the conductance distribution shows stronger deviation from its limiting case of uncorrelated equivalent channels (dashed lines) than the width distribution does.

Figure 4 shows the case of asymmetric leads for the asymmetry factor $a = 1$ and 10, for four-point leads with $k|\Delta \boldsymbol{r}| = 1$, and for both the orthogonal and the unitary limits. $P(g)$ is not very sensitive to the lead's asymmetry and a large value of a is needed to see significant variation from the symmetric lead's case. In the limit $a \to \infty$, one can neglect the smaller width in Eq. (1) and the conductance peak g is proportional to the partial width in the dominating lead. In this limit $P(g)$ is reduced to $P(\Gamma)$ shown by the dashed lines in Fig. 4. The asymmetry effect becomes larger for an increasing number of channels (this effect can be noticed by comparing the GOE and GUE cases, since for the same number of physical channels Λ the GUE has a larger number of ''effective'' channels).

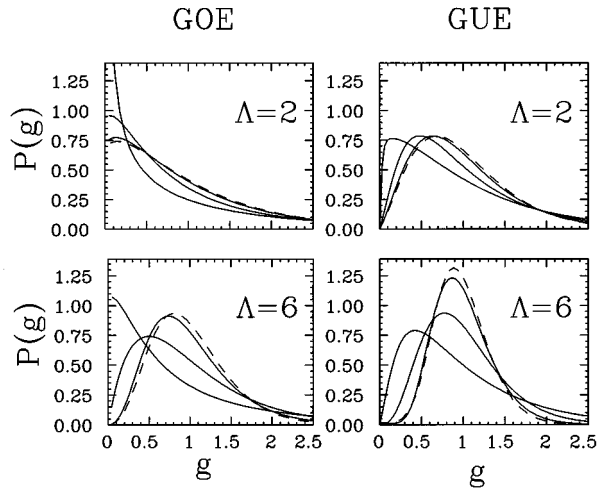

FIG. 3. Same as Fig. 2 but for the conductance peak distributions $P(g)$ in dots with symmetric Λ-point leads.

IV. DYNAMICAL MODEL

To test the RMT predictions for the statistical distributions, we modeled a quantum dot by a system whose classical dynamics is chaotic. The chosen model is the conformal billiard,[19,38] whose shape is defined by the image of the unit circle in the complex z plane under the conformal mapping

$$w(z) = \frac{z + bz^2 + ce^{i\delta} z^3}{\sqrt{1 + 2b^2 + 3c^2}}. \tag{34}$$

The parameters b, c, and δ control the billiard shape. Equation (34) ensures that the area $\mathcal{A}$ enclosed by $w(z)$ is normalized to π and is independent of the shape. The billiard characterized by $c = 0$ is known as the Africa billiard. We analyze the case $b = 0.2$, $c = 0.2$, and $\delta = \pi/2$, for which the classical dynamics is known to be chaotic.[20] We have verified that the corresponding spectrum exhibits GOE-like spectral fluctuations (we used 300 converged levels by diagonalizing a matrix of order 1000). This is demonstrated in Fig. 5, where the nearest-neighbor level spacing distribution $P(s)$ and the Δ_3 statistics, which measures the spectral rigidity, are shown.

To investigate the effect of an external magnetic field, we consider the same billiard threaded by an Aharonov-Bohm flux line,[38,20] which does not affect the classical dynamics. The flux is parametrized by $\Phi = \alpha \Phi_0$, where Φ_0 is the unit flux. We use the same set of values for b, c, and δ as above

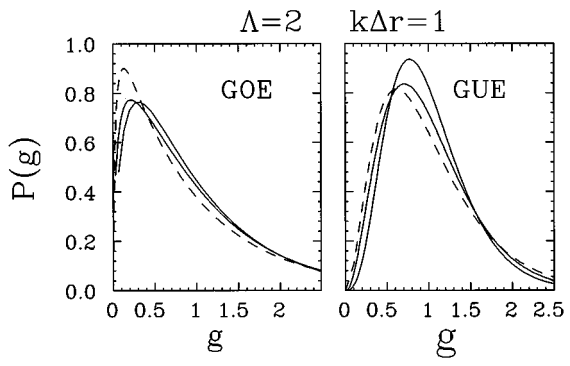

FIG. 4. Conductance peak distributions $P(g)$ for asymmetric four-point leads with $k|\Delta \boldsymbol{r}| = 1$ and an asymmetry factor of $a = 1$ and $a = 10$. Left: GOE; right: GUE. The dashed curves describe the limit $a \to \infty$ where $P(g)$ reduces to $P(\Gamma)$.

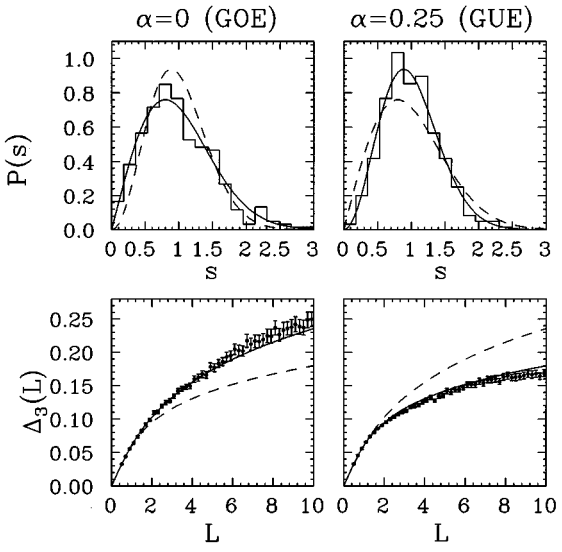

FIG. 5. The nearest-neighbor level spacing distribution $P(s)$ and the Δ_3 statistics for the conformal billiard with $b=0.2$, $c=0.2$, and $\delta=\pi/2$. We consider the states between the 50th and the 350th. Left: no magnetic flux ($\alpha=0$). Right: with magnetic flux $\alpha=1/4$.

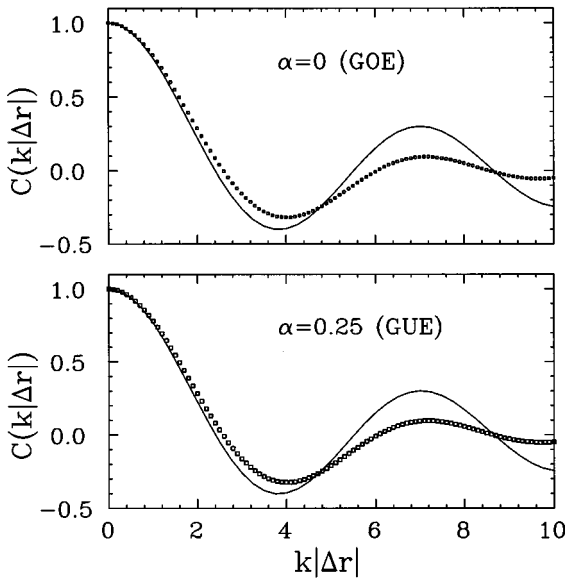

FIG. 6. The spatial wave-function correlation $C(k|\Delta\boldsymbol{r}|)$ calculated for the conformal billiard (squares) compared with the theoretical prediction $J_0(k|\Delta\boldsymbol{r}|)$ (solid line). The top panel corresponds to $\alpha=0$ and the bottom panel to $\alpha=1/4$.

(to ensure classical chaotic motion), and choose $\alpha=1/4$ for maximal time-reversal symmetry breaking. The statistical tests shown in Fig. 5 confirm that this choice of α corresponds to the unitary limit. We remark that the Δ_3 statistics is a better measure to distinguish between the GOE and GUE cases than the level spacing distribution $P(s)$ (used in Ref. 20).

A. Spatial correlations

The eigenfunction amplitude correlation $C(k|\Delta\boldsymbol{r}|)=\overline{\Psi^*(\boldsymbol{r})\Psi(\boldsymbol{r}')}/\overline{|\Psi(\boldsymbol{r})|^2}$ was recently investigated thoroughly for the conformal billiard.[31] The results agree fairly well with the theoretical prediction, namely, $C(k|\Delta\boldsymbol{r}|)=J_0(k|\boldsymbol{r}-\boldsymbol{r}'|)$,[30] if one averages over the orientation of $\Delta\boldsymbol{r}$. This result is based on semiclassical arguments, and the eigenfunctions studied in Ref. 31 were chosen accordingly to be highly excited states (i.e., deep in the semiclassical region).

To apply this result to quantum dots, further considerations are in order. First, a typical semiconductor quantum dot in the submicrometer range contains several hundred electrons, and it is therefore not obvious that the eigenstates around the Fermi level are necessarily semiclassical. Second, scars associated with isolated periodic orbits give corrections to $C(k|\Delta\boldsymbol{r}|)$ that are of order $O(\hbar^{1/2})$. The fluctuations of the spatial correlation of the billiard eigenfunctions were recently estimated analytically[39] and found also to be suppressed by $O(\hbar^{1/2})$. These corrections are negligible if one averages over all orientations around a given point $\boldsymbol{r}$ (keeping the modulus $|\Delta\boldsymbol{r}|$ fixed), but this is difficult to implement experimentally. At a fixed orientation the fluctuations of the spatial correlations seem to be rather small (in comparison with the average correlator) if $k|\Delta\boldsymbol{r}|\leqslant 3$ so that Eq. (19) is a good approximation. For larger values of $k|\Delta\boldsymbol{r}|$, there could be significant fluctuations from Eq. (19), but for such values of $k|\Delta\boldsymbol{r}|$ the width and conductance distributions are closer to their limiting case of independent channels and are not very sensitive to the exact correlations.

Our results were obtained by using the billiard eigenfunctions with Neumann boundary conditions where the normal derivative of the wave-functions vanishes on the boundaries. We analyze eigenfunctions in the vicinity of the 100th excited level, which resembles the experimental situation. By moving the points around the circle we generate more statistics and average over orientations. The results are shown in Fig. 6 where the correlations in the model (solid line) compare well with the theoretical result (dashed line) for both cases with and without magnetic flux. The agreement is reasonable, particularly for $k|\Delta\boldsymbol{r}|<5$ (no average over orientation is made). For $k|\Delta\boldsymbol{r}|\gg 1$, the deviations from the theoretical value of $C(k|\Delta\boldsymbol{r}|)$ are not important since the channels are weakly correlated and the distributions are very close to those describing uncorrelated channels. Thus, corrections to our analytical findings should not be large, as is supported by the numerical evidence presented below.

We remark that in order to simplify the calculations we used Neumann boundary conditions around the entire billiard's boundary and not just at the dot-lead interface. To resemble the experimental situation we would have to use mixed boundary conditions,[20] which would make the calculations much more computationally intensive. However, while the actual values of the eigenfunctions depend on the boundary conditions, the eigenfunctions' statistics does not and our simplified calculations are sufficient.

B. Coupling to leads and distributions

We first studied the pointlike contact model by describing the lead as a sequence of Λ equally spaced points on the

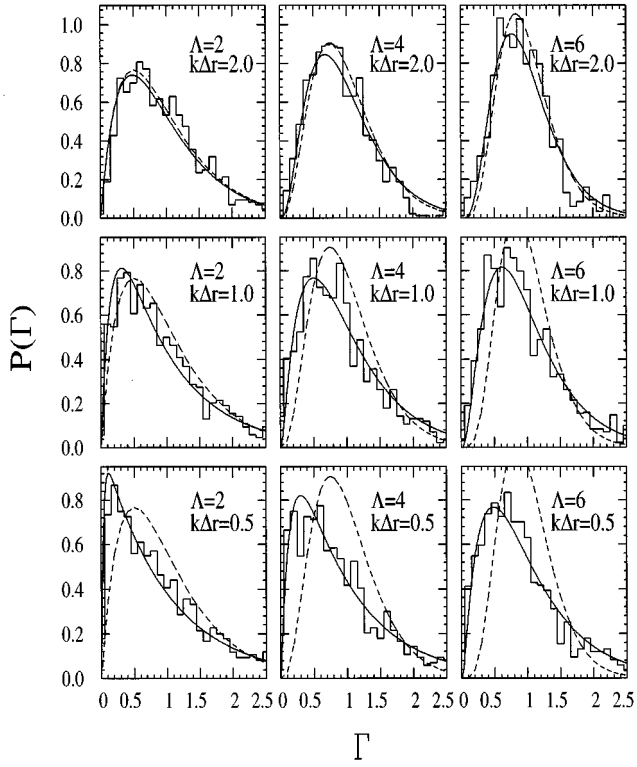

FIG. 7. Total width distributions $P(\Gamma)$ for broken time-reversal symmetry (GUE) for several values of $k|\Delta \boldsymbol{r}|=0.5,\ 1,\ 2$ and for various number of channels $\Lambda=2,\ 4,\ 6$. The solid lines are the theoretical distributions (23), while the dashed lines correspond to uncorrelated and equivalent channels. The histograms are the results from the conformal billiard ($b=0.2,\ c=0.2,\ \delta=\pi/2$) where a magnetic flux line ($\alpha=1/4$) breaks time-reversal symmetry.

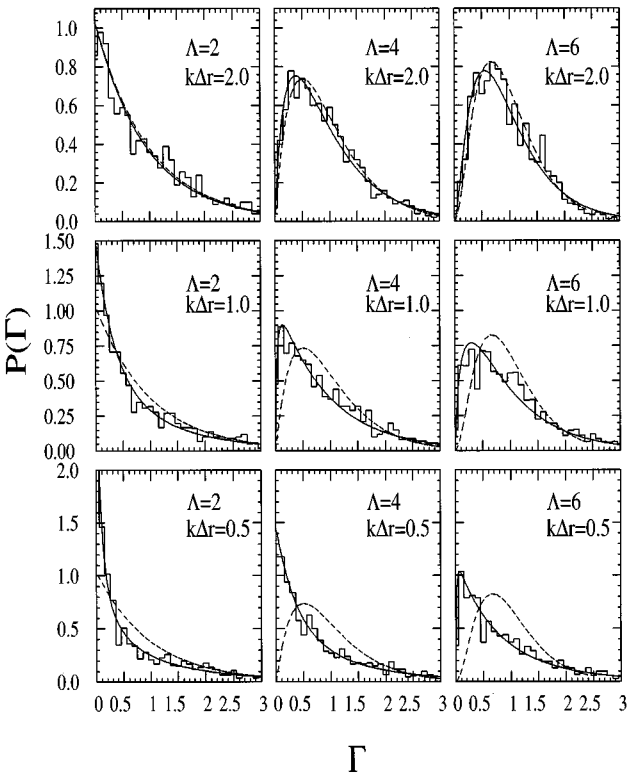

FIG. 8. Total width distributions $P(\Gamma)$ for conserved time-reversal symmetry (GOE). Conventions are as in Fig. 7 but with solid lines describing the orthogonal prediction (27). The conformal billiard has no magnetic flux line ($\alpha=0$).

boundary of the billiard (in the w plane). According to Eq. (19) the correlation matrix M is then completely determined by $k|\Delta \boldsymbol{r}|\approx k\,\delta\theta|w'(r=1,\theta)|$ (where $\delta\theta$ is the angle that spans the arc between two neighboring points in the z plane) and Λ. In this model it is easy to generate strong correlations by choosing the points close enough (i.e., the distance is chosen to be shorter than the Fermi wavelength). This should be contrasted with the (discretized) Anderson model[12] where the channels are weakly correlated even if the lead is composed of nearest-neighboring points. The eigenvalues w_c^2 are found by diagonalizing the matrix M.

In Figs. 7 and 8 we compare, for both the unitary and orthogonal limits, respectively, the total width distribution $P(\Gamma)$ in the conformal billiard (histograms) with the theoretical predictions (solid lines). This is done for several values of $k|\Delta \boldsymbol{r}|=0.5,\ 1,\ 2$ and $\Lambda=2,\ 4,\ 6$. The case of equivalent and uncorrelated channels (displayed by dashed lines) is just the χ^2 distributions in Λ (2Λ) degrees of freedom for the GOE (GUE). The agreement between the model and the analytic RMT predictions confirms the validity of the statistical model for a chaotic dot. We observe from Figs. 7 and 8 that for the larger values of $k|\Delta \boldsymbol{r}|$, the distributions get closer to those for uncorrelated channels. This is consistent with the decrease in spatial correlations (see Fig. 6). Another interesting observation is that, for a constant $k|\Delta \boldsymbol{r}|$ (i.e., fixed correlations), the deviation from the limiting case of independent channels becomes larger with an increasing number of channels.

Figures 9 and 10 show a comparison between the theoretical conductance peak distributions for symmetric leads, as given by Eqs. (32) and (33) for the unitary and orthogonal cases, respectively, and those calculated for the conformal billiard with symmetric Λ-point leads ($\Lambda=2,\ 4$, and 6) and for different values of $k|\Delta \boldsymbol{r}|$. The dashed lines are again the limiting case of uncorrelated and equivalent leads. Observations can be made with respect to the conductance peak distributions that are similar to the ones made above for the width distributions. Comparing the width and conductance peak distributions, we note that the conductance distribution shows stronger deviation from its limit for uncorrelated equivalent channels than does the width distribution.

We also studied extended leads by taking the contact region of the lead and the dot to have a finite length $D\approx|w'|\Delta\theta$ on the dot's boundary (in the w plane) where w' is evaluated at the corresponding angle where the lead is located. In this case the channels are defined by the allowed quantized transverse momenta $\kappa_c=\pi n_c/D$ with $n_c=1,2,\ldots,\Lambda$, where $\Lambda=\mathrm{int}[kD/\pi]$. To calculate the partial amplitude for the conformal billiard, the integral in Eq. (2) (defined in the w plane) is mapped into an integral along an arc in the z plane, which is spanned by an angle $\Delta\theta$:

$$\gamma_{c\lambda}=\sqrt{\frac{\hbar^2}{2m}}\int_{\Delta\theta}d\theta|w'(r=1,\theta)|\Phi_c^*(\theta)\Psi_\lambda(r=1,\theta). \qquad (35)$$

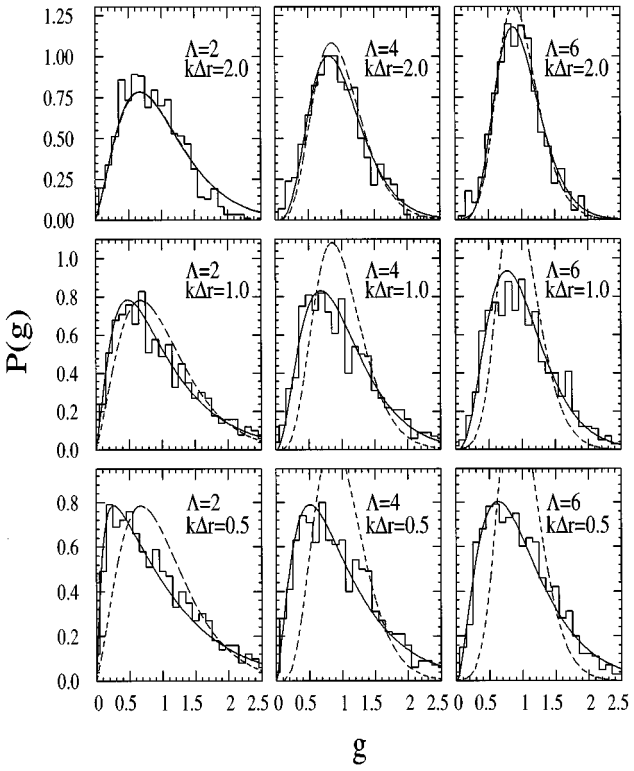

FIG. 9. Conductance peak distributions $P(g)$ for broken time-reversal symmetry (GUE). The histograms display the results obtained from the conformal billiard for symmetric Λ-point leads and different values of $k|\Delta \boldsymbol{r}|$. The solid lines are the RMT prediction (32) and the dashed lines correspond to uncorrelated and equivalent channels. The cases presented are the same as in Fig. 7.

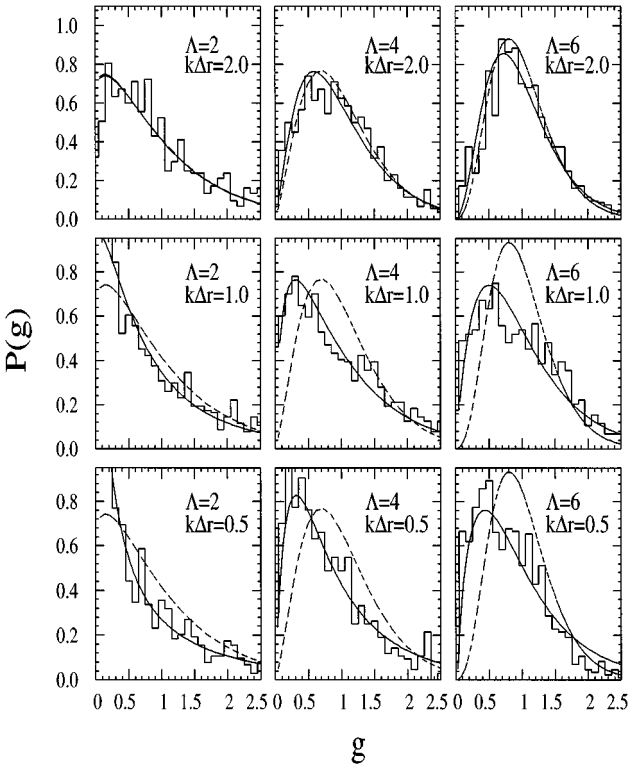

FIG. 10. Same as Fig. 9 but for the orthogonal symmetry where the theoretical distribution is given by Eq. (33). The results for the conformal billiard correspond to $\alpha=0$.

Here $\Phi_c(\theta)=\sqrt{2/D}\sin(\kappa_c|w'|\theta)$ are the transverse channel wave-functions and for simplicity we have set $k_c P_c=1$. The resonance eigenfunction Ψ_λ is given in terms of its expansion in $e^{il\theta}$ (with $l=0,\pm1,\pm2,\ldots$)

$$\Psi_\lambda(r=1,\theta)=\mathcal{N}_\lambda\sum_j \frac{c_j^\lambda}{\sqrt{\pi(\gamma_j^2-|\not{\ell}_j-\alpha|^2)}}e^{i\not{\ell}_j\theta}, \quad (36)$$

where $\mathcal{N}_\lambda$ is a normalization constant, γ_j are the zeroes of $J'_{|\not{\ell}_j-\alpha|}$, and c_j are expansion coefficients as in Ref. 20.

To guarantee that the correlation matrix M in Eq. (10) is the same for eigenfunctions of the billiard that belong to different energies, we choose D such that $kD=\text{const}$ and scale the partial amplitude (2) by $k^{1/2}$. The resulting matrix is

$$kM_{cc'}=\frac{\hbar^2}{2m}\frac{2}{kD}\int_{\Delta\theta}d\theta\int_{\Delta\theta}d\theta'|w'(r=1,\theta)||w'(r=1,\theta')|$$
$$\times\sin\left(\frac{\pi n_c}{kD}|w'|\theta\right)J_0(|w'||\theta-\theta'|)$$
$$\times\sin\left(\frac{\pi n_{c'}}{kD}|w'|\theta'\right). \quad (37)$$

This scaling has the advantage of being consistent with the theoretical approach presented above, but experimentally it is difficult to accomplish. Fortunately, this scaling of D is insignificant for current experiments[14,15] that deal with dots containing several hundred electrons $\mathcal{N}$. Indeed, from the Weyl formula we have $k_F\propto\mathcal{N}^{1/2}$ so that $\delta k_F/k_F=\delta\mathcal{N}/2\mathcal{N}\ll1$. The latter inequality is obtained when we estimate $\delta\mathcal{N}$ to be the number of observed Coulomb blockade peaks (since each Coulomb blockade peak corresponds to the addition of one electron into the dot). The relative variation of k_F is thus small and can be neglected.

We find that the channels in the extended leads model are weakly correlated and that the average partial widths in the various channels exhibit a moderate variation. In such a case the total width distribution is not very different from the case of uncorrelated equivalent channels. Our model calculations for extended leads are shown in Fig. 11 and are in agreement with the RMT predictions for uncorrelated channels (dashed lines). An interesting effect is that with an increasing number of channels even small deviations in $P(\Gamma)$ give rise to relatively large deviations in $P(g)$.

V. CONNECTION TO EXPERIMENTS AND CONCLUSIONS

We have discussed the cases of both orthogonal and unitary symmetries. To relate to actual experimental situations, it is important to estimate the minimal strength of the magnetic field B_c, which ensures complete time-reversal symmetry breaking. For a ballistic electron[38,8,20,40] $B_c\mathcal{A}\propto\sqrt{\tau_{\rm cr}/\tau}\Phi_0$, where $\tau_{\rm cr}$ is the time it takes the electron to cross the dot and τ is the Heisenberg time $\tau=h/\Delta$. For an electron at the Fermi energy $B_c\mathcal{A}\propto\mathcal{N}^{-1/4}\Phi_0$, where $\mathcal{N}$ is the number of electrons in the dot. The proportionality factor is

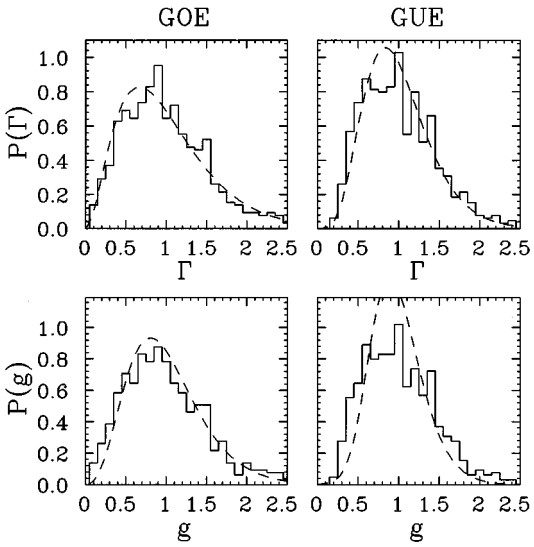

FIG. 11. Comparison of conformal billiard results for extended leads with $\mathrm{int}[kD/\pi]=6$ (histograms) and theoretical predictions. Shown are the total width distribution $P(\Gamma)$ (top) and the conductance distribution $P(g)$ (bottom) for both orthogonal (left) and unitary (right) limits. The dashed lines correspond to uncorrelated equivalent channels.

nonuniversal and depends on the exact geometry of the dot. In a semiclassical analysis[41,42] it can be expressed in terms of classical quantities. Typical values of B_c in some recent experiments[14,15] are of the order of a few mT. Such small values of B_c are in the range where classical perturbation theory is valid, and the leading semiclassical correction to any two-point correlator is the change in magnetic flux through the area enclosed by the classical trajectory, while the bending of the trajectory itself is second order.[41] For larger magnetic fields, when this is no longer valid, the physics is different and in particular the classical motion begins to be regular. Using the same reasoning, the assumption that the correlator $C(k|\Delta \boldsymbol{r}|)$ is unchanged by the magnetic field is strictly valid only for the regime where classical perturbation applies. Nevertheless, it is noteworthy that these small variations in the magnetic field lead to appreciable quantum mechanical effects, i.e., the crossover from orthogonal to unitary symmetry.

In conclusion, we have derived closed expressions for the width and conductance peak distributions in quantum dots in the Coulomb blockade regime. The main assumption is that for a ballistic dot the irregular boundary gives rise to chaotic motion. For given correlation matrices that characterize the left and right leads, these distributions are universal and distinct for conserved and broken time-reversal symmetry. While recent experiments have measured the conductance distributions in symmetric one-channel leads, it would be interesting to measure and compare with theory the conductance distributions in dots with multichannel leads.

ACKNOWLEDGMENTS

This work was supported in part by the U.S. Department of Energy Grant No. DE-FG02-91ER40608. C.H.L. acknowledges financial support by the Conselho Nacional de Pesquisas (CNPq Brazil). We thank H. U. Baranger and A. D. Stone for discussions and H. Bruus for the use of his billiard computer program.

[1] C. M. Marcus, A. J. Rimberg, R. M. Westervelt, P. F. Hopkins, and A. C. Gossard, Phys. Rev. Lett. **69**, 506 (1992).
[2] See, for example, M. A. Kastner, Rev. Mod. Phys. **64**, 849 (1992).
[3] U. Meirav, M. A. Kastner, and S. J. Wind, Phys. Rev. Lett. **65**, 771 (1990).
[4] E. B. Foxman, P. L. McEuen, U. Meirav, N. S. Wingreen, Y. Meir, P. A. Belk, N. R. Belk, M. A. Kastner, and S. J. Wind, Phys. Rev. B **47**, 10 020 (1993).
[5] E. B. Foxman, U. Meirav, P. L. McEuen, M. A. Kastner, O. Klein, P. A. Belk, D. M. Ambusch, and S. J. Wind, Phys. Rev. B **50**, 14 193 (1994).
[6] C. E. Porter, *Statistical Theory of Spectra: Fluctuations* (Academic Press, New York, 1965).
[7] C. H. Lewenkopf and H. A. Weidenmüller, Ann. Phys. (N.Y.) **212**, 53 (1991); C. H. Lewenkopf and H. A. Weidenmüller, Phys. Rev. Lett. **68**, 3511 (1992).
[8] R. A. Jalabert, A. D. Stone, and Y. Alhassid, Phys. Rev. Lett. **68**, 3468 (1992).
[9] E. P. Wigner and L. Eisenbud, Phys. Rev. **72**, 29 (1947).
[10] A. M. Lane and R. G. Thomas, Rev. Mod. Phys. **30**, 257 (1958).
[11] V. N. Prigodin, K. B. Efetov, and S. Iida, Phys. Rev. Lett. **71**, 1230 (1993).
[12] E. R. Mucciolo, V. N. Prigodin, and B. L. Altshuler, Phys. Rev. B **51**, 1714 (1995).
[13] K. B. Efetov, Adv. Phys. **32**, 53 (1983).
[14] A. M. Chang, H. U. Baranger, L. N. Pfeiffer, K. W. West, and T. Y. Chang, Phys. Rev. Lett. **76**, 1695 (1996).
[15] J. A. Folk, S. R. Patel, S. F. Godijn, A. G. Huibers, S. M. Cronenwett, C. M. Marcus, K. Chapman, and A. C. Gossard, Phys. Rev. Lett. **76**, 1699 (1996).
[16] I. H. Chan, R. M. Clarke, C. M. Marcus, K. Chapman, and A. C. Gossard, Phys. Rev. Lett. **74**, 3876 (1995).
[17] H. U. Baranger and P. A. Mello, Phys. Rev B. **51**, R4703 (1995); P. W. Brouwer and C. W. J. Beenakker, *ibid.* **51**, 7739 (1995).
[18] Y. Alhassid and C. H. Lewenkopf, Phys. Rev. Lett. **75**, 3922 (1995).
[19] M. Robnik, J. Phys. A **16**, 3971 (1983); **17**, 1049 (1983).
[20] H. Bruus and A. D. Stone, Phys. Rev. B **50**, 18275 (1994); Physica B **189**, 43 (1993).
[21] H. Alt, H.-D. Gräf, H. L. Harney, R. Hofferbert, H. Lengerer, A. Richter, P. Schardt, and H. A. Weidenmüller, Phys. Rev. Lett. **74**, 62 (1995).
[22] J. Stein and H.-J. Stöckmann, Phys. Rev. Lett. **68**, 2867 (1992); J. Stein, H.-J. Stöckmann, and U. Stoffregen, *ibid.* **75**, 53 (1995).
[23] S. Sridhar, Phys. Rev. Lett. **67**, 785 (1991); A. Kudrolli, V. Kidambi, and S. Sridhar, Phys. Rev. Lett. **75**, 822 (1995).
[24] C. W. J. Beenakker, Phys. Rev. B **44**, 1646 (1991).
[25] M. R. Zirnbauer, Nucl. Phys. **A560**, 95 (1993).
[26] H.-J. Sommers and S. Iida, Phys. Rev. E **49**, R2513 (1994); V. I.

Fal'ko and K. B. Efetov, Phys. Rev. B **50**, 11 267 (1995).
[27] T. A. Brody, J. Flores, J. B. French, P. A. Mello, A. Pandey, and S. S. M. Wong, Rev. Mod. Phys. **53**, 385 (1981).
[28] T. J Krieger and C. E. Porter, J. Math. Phys. **4**, 1272 (1963); N. Ullah, *ibid.* **4**, 1279 (1963).
[29] See, for example, in N. N. Lebedev, *Special Functions and their Applications* (Dover, New York, 1972).
[30] M. V. Berry, J. Phys. A **10**, 2083 (1977).
[31] B. Li and M. Robnik, J. Phys. A **27**, 5509 (1994).
[32] The dynamical model analyzed in this paper is not relevant for this discussion, since the time-reversal symmetry is broken by a Bohm-Aharonov flux line, which does not change the classical trajectories at all.
[33] V. N. Prigodin, Phys. Rev. Lett. **74**, 1566 (1995); V. N. Prigodin, N. Tanigushi, A. Kudrolli, V. Kidambi, and S. Sridhar, *ibid.* **75**, 2392 (1995).
[34] M. Srednicki, Phys. Rev. E **54**, 954 (1996).
[35] There have been several experimental efforts to accumulate sufficient statistics for $P(\Gamma)$ in compound nucleus reactions; see, for example S. F. Mughabghab, M. Divadeenam, and N. E. Holden, *Neutron Resonance Parameters and Thermal Cross Sections* (Academic Press, New York, 1981). However, the statistics was relatively poor and the correlation mechanism for M is of a different nature than the one discussed here.
[36] Y. Alhassid and R. D. Levine, Phys. Rev. Lett. **57**, 2879 (1986); Y. Alhassid and M. Feingold, Phys. Rev. A **39**, 374 (1989).
[37] The corresponding condition is $kL \gg 1$, where L is the distance between the leads (a typical dot's size). It is hard to estimate the corrections of order $(kL)^{-1}$ to our results, and one might expect that they would impose limitations on our analytical findings. Fortunately the numerical results presented in the next section show that such corrections are indeed very small.
[38] M. V. Berry and M. Robnik, J. Phys. A **19**, 649 (1986).
[39] M. Srednicki and F. Stiernelof, J. Phys. A **29**, 5817 (1996).
[40] K. Frahm and J.-L. Pichard, J. Phys. I (France) **5**, 847 (1995).
[41] O. Bohigas, M.-J. Giannoni, A. M. Ozório de Almeida, and C. Schmit, Nonlinearity **8**, 203 (1995).
[42] Z. Pluhař, H. A. Weidenmüller, J. A. Zuk, C. H. Lewenkopf, and F. J. Wegner, Ann. Phys. (N.Y.) **253**, 1 (1995).